Incorporation of Counter Ions in Organic Molecules: New Strategy in Developing Dopant-Free Hole Transport Materials for Efficient Mixed-Ion Perovskite Solar Cells

Jinbao Zhang,[a‖] Bo Xu,[b‖] Li Yang,[c] Alba Mingorance,[d] Changqing Ruan,[c] Yong Hua,[e] Linqin Wang,[b] Nick Vlachopoulos,[f] Mónica Lira-Cantú,[d] Gerrit Boschloo,[a] Anders Hagfeldt, [a, f] Licheng Sun[b], Erik M. J. Johansson [a*]*

Dr. J. Zhang, Dr. G. Boschloo, Dr. E. M. J. Johansson
[a] Physical Chemistry, Center of Molecular Devices, Department of Chemistry–Ångström Laboratory, Uppsala University, SE-75120, Uppsala, Sweden
Email: erik.johansson@kemi.uu.se

Dr. B. Xu, L. Wang, Prof. L. Sun
[b] Organic Chemistry, Center of Molecular Devices, Department of Chemistry, Chemical Science and Engineering, KTH Royal Institute of Technology, SE-10044, Stockholm, Sweden.
Email : lichengs@kth.se

Dr. L. Yang, C. Ruan
[c] Nanotechnology and Functional Materials, Department of Engineering Science, Uppsala University, SE-75120, Uppsala, Sweden

A. Mingorance, Prof. M. Lira-Cantú
[d] Catalan Institute of Nanoscience and Nanotechnology (ICN2), Campus UAB, Bellaterra, 08193 Barcelona, Spain

Dr. Y. Hua,
[e] Applied Physical Chemistry, Center of Molecular Devices, Department of Chemistry, KTH-Royal Institute of Technology, Teknikringen 30, SE-10044 Stockholm, Sweden

Dr. N. Vlachopoulos, Prof. A. Hagfeldt
[f] Laboratory of Photomolecular Science, Institute of Chemical Sciences and Engineering, École Polytechnique Fédérale de Lausanne, EPFL-FSB-ISIC-LSPM, Chemin des Alambics, Station 6, CH-1015, Lausanne, Switzerland

Key words: dopant free, ionic hole transport material, mixed ion perovskite, counter ions, high efficiencies.

Dr. J. Zhang and Dr. B. Xu contributed this work equally.

Organic-inorganic hybrid perovskites, with a formula of ABX_3, (A: cations, B: Pb, X: halides), have recently attracted great attention in the solar-cell community for being efficient light absorbers. These perovskites show excellent physical and optoelectronic properties, such as ambipolar charge-carrier transport, long carriers diffusion length, strong panchromatic light absorption and they are also solution processable.[1-3] The perovskite-based solar cell (PSC) has demonstrated impressive performance by showing an increase of the power conversion efficiency (PCE) from 3% to a certified 22% during the past few years.[4] The great success of PSCs is significantly attributed to the tremendous efforts in the perovskite compositional engineering, device-architecture design, solar-cell stability improvement and charge-selective layer optimization.[5-9] Designing new low-cost and efficient hole transport materials (HTMs) has attracted great interest from many research groups.[10-12] The motivation is justified by the fact that the preparation of the established state-of-the-art molecular HTM 2,2',7,7'-tetrakis-(N,N-di-p-methoxy-phenyl-amine) 9,9'spiro-bifluorene (spiro-OMeTAD) presents tedious synthetic steps; thus this material is very expensive with a price more than 10 times than that of Gold or Platinum.[13] The high cost and relatively low hole conductivity of spiro-OMeTAD significantly limits its realistic large-scale application although it is so far the most commonly used HTM with outstanding performance in PSCs.[14] The key function of the HTM layer in PSCs is to accept the holes from the photoexcited perovskite at the interfaces and to conduct the holes towards the contact; therefore, the HTM layer has a great impact on the charge extraction in the device.[15] In this regards, high hole conductivity is one of the most primary parameters which should be considered in the design of the new HTMs. Generally organic small molecules have relatively low hole conductivities, for example ~10^{-5} Scm^{-1} for undoped spiro-OMeTAD.[16] During the operation of the PSC under illumination, a large amount of the photoinduced holes from the perovskite layer inject into the HTM layer after light excitation, followed by hole conduction through the HTM layer. During this process, rather high quantities of holes (oxidized HTM molecules) and negatively charged counter ions in HTM are highly desired in order to enhance the hole conductivity of the HTM. In this context, doping of the organic molecular HTM by chemical oxidants is an effective way to enhance the HTM hole conductivity. For example, Burschka, *et al.*, used a cobalt-complex, coded as FK209, as dopant in order to oxidize spiro-OMeTAD for solid-state dye-sensitized solar cells (ssDSSCs), and an impressive efficiency of 7.2% was achieved.[13] Currently the

dopant FK209 together with LiTFSI [bis(trifluoromethane)sulfonimide lithium salt] and *tert*-butyl pyridine has been commonly applied in most of high-efficiency PSCs. In addition, Xu, *et al.,* developed AgTFSI as a new type of dopant and applied it successfully in the ssDSSCs and PSCs.[17] Snaith, *et al.*, demonstrated that LiTFSI can be a doping agent for the HTM in the presence of O_2-containing atmosphere.[18] In the doping process, the counter ions are required to compensate the positively charged HTM, such as spiro-OMeTAD$^+$. In this respect, the salt LiTFSI is usually added in the HTM solution before the HTM deposition. However, it has been reported that the introduced additives in the HTM could cause severe device instability,[19] because some components, for instance LiTFSI, are hydrophilic and this can be the cause of the moisture-induced perovskite degradation.[13] Besides, it is extremely challenging to precisely control the doping density in this poorly-defined oxidative process, and therefore difficulties arise with respect to device reproducibility.[20] In this regard, developing dopant-free HTM is critical for making efficient and stable PSCs. To date, there are several reports on dopant-free HTMs for PSCs. For instance, Liao and coworkers designed a dopant-free polymer as HTM and a PCE of 12.3% was achieved. Fei *et al.*, developed several star-shaped triphenylamine (TPA)-based dopant-free HTMs and the device based on the optimal of them exhibited a PCE of 15.4%. [21] Other TPA-based dopant-free HTMs have been applied in PSCs by Li and coworkers, obtaining PCEs of 11-13%.[22-24] Steck *et al.*, developed A-D-A-type S, N-heteropentacene-based dopant-free HTM and obtained 10.3-11.4%.[25] Liu *et al.*, reported a tetrathiafulvalene derivative, TTF-1, as dopant-free HTM with a PCE of 11.0% was achieved.[26] Recently, Kim et al., reported dopant-free polymeric HTM in PSC with a high PCE of 17.3%.[27] Although different types of molecules or polymers have been designed to be used as dopant-free HTMs, the reported efficiencies of the PSCs based on them are still much lower than those with properly doped HTMs. Besides, there is lack of effective design strategies for guiding the future development of new dopant-free HTMs.

Here, we have introduced a new strategy for developing a new-type ionic organic molecule, X44 (see **Figure 1**), as dopant-free HTM for PSCs. To the best of our knowledge, this is for the first time the incorporation of counter ions directly in the organic molecules as HTM in PSCs is reported. The device based on X44 without any dopants and additives exhibited a promising PCE of 16.2% after aging for 15 days from an initial PCE of 15.2%, in comparison to two reference molecules AS37 (7.8%) and X41(<0.1%). We found that the

introduced counter ions in the molecules play an important role in the hole conductivity property, HTM film formation, interfacial hole transfer yield, as well as device stability. We believe that this new strategy of designing ionic organic HTM promises to pave the way to the future efficient design of new dopant-free HTMs for PSCs.

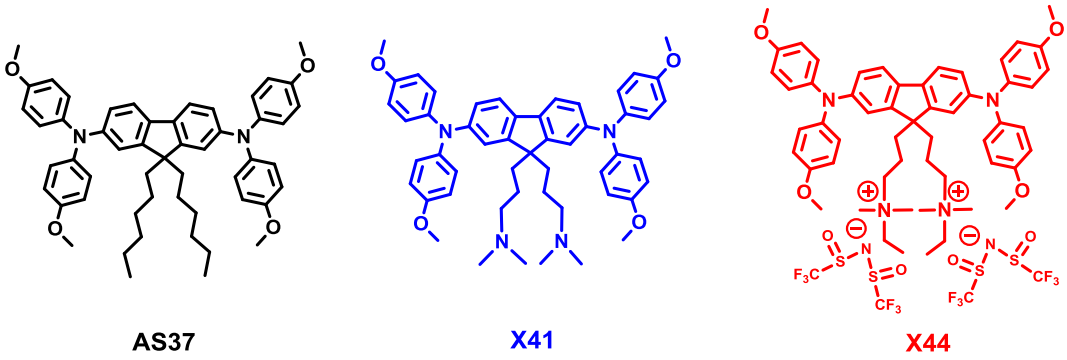

Figure 1. Chemical structures of HTMs: AS37, X41 and X44.

The chemical structures of AS37, X41 and X44 are depicted in **Figure 1**. The tail end of the alkyl chains shown in AS37 has been modified in X41 by attaching tertiary amine groups, and further in X44 to quaternary ammonium coupled with associated counter ions $TFSI^-$. The detailed HTM synthesis (**Scheme S1**) and characterization (**Figure S1-S6**) are shown in Supporting Information. By this novel design, the anion $TFSI^-$ is successfully incorporated into the molecule X44. As discussed above, the incorporated counter ions may have a significant impact on the hole conduction process. Therefore, we investigated the possibility of using this quaternary ammonium salt as dopant-free HTM in PSCs and systematically studied the influence of the structural modulations in these three HTMs on their molecular properties and the photovoltaic performance in PSCs.

Firstly, the optoelectronic properties of three HTMs were characterized. The UV-vis absorption spectra of the three molecules dissolved in CH_2Cl_2 are displayed in **Figure** S7 and summarized in **Table 1**. As shown, all three HTMs showed very similar maximum absorption peaks, although the λ_{max} for X44 was slightly blue-shifted, at 381 nm, compared to X41 (λ_{max}=383nm) and AS37 (λ_{max}=385nm). It can be concluded that the alkyl chain in AS37 compared to the tertiary amine in X41 and quaternary ammonium in X44 has little influence on their optical absorption property. From the onset absorption wavelength we could extract the bandgaps of AS37, X41 and X44 at 2.95, 2.97 and 2.94 eV, respectively.

To evaluate the energy levels of the HTMs, cyclic voltammetry of HTMs in CH_2Cl_2 was performed for three molecules, as displayed in **Figure S7**. The

HOMO levels of the molecules were extracted from the first-electron redox potentials and listed in **Table 1**. A slightly down-shifted trend in E_{HOMO} was demonstrated, from -4.99 eV, through -5.01 eV to -5.02 eV for AS37, X41 and X44, respectively. It can therefore be concluded that the change of the molecular structure does not significantly affect the band structures. The similar HOMO levels for three HTMs also indicate that comparable open-circuit voltage (V_{oc}) values are expected for the devices based on AS37, X41 and X44 if they present similar charge extraction and charge-recombination kinetics.

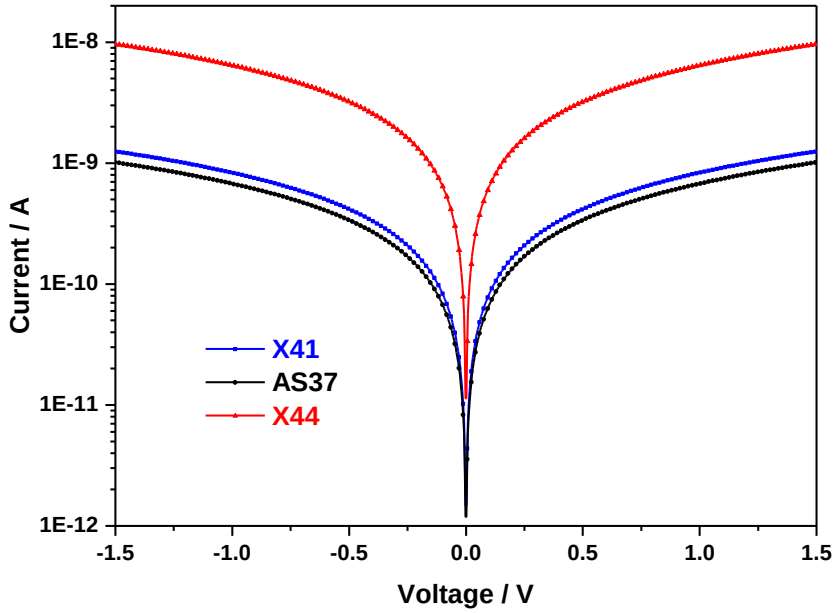

Figure 2. Hole conductivity of the HTMs AS37 (black curve), X41 (blue curve) and X44 (red curve).

As discussed above, the hole conductivity is a critical factor for determining the potential usability of these new HTMs in PSCs, since the hole conductivity can significantly affect the hole collection in the device. The hole conductivity measurements were performed by using a two-contact electrical conductivity setup.[16] The obtained *I-V* curves are shown in **Figure 2**, and the calculated hole conductivities for different HTMs are summarized in **Table 1**. It can be seen that X44 exhibited a much higher hole conductivity (9.03×10^{-4} S cm^{-1}), more than 10 times higher than that of AS37 (7.65×10^{-5} Scm^{-1}) and X41 (8.95×10^{-5} Scm^{-1}). In comparison, the standard undoped spiro-OMeTAD has a conductivity of 8.67×10^{-5} Scm^{-1} which was measured by using the same method.[16] This demonstrates that the introduced counter ions in the HTM X44 can significantly enhance the hole conductivity, which will be highly beneficial to the device performance in terms of the charge extraction.

Table 1. Summary of the optical, electrochemical and photoelectric properties of HTMs

HTM	λ_{max} [a] [nm]	$E_{0\text{-}0}$ [b] [eV]	E_{HOMO} [c] [eV]	E_{LUMO} [d] [eV]	Hole conductivity [S cm^{-1}]
AS37	300, 385	2.95	-4.99	-2.04	7.65×10^{-5}
X41	301, 383	2.97	-5.01	-2.04	8.95×10^{-5}
X44	302, 381	2.94	-5.02	-2.08	9.03×10^{-4}
Spiro-OMeTAD	-	-	-5.10	-	8.76×10^{-5} [ref.16]

[a] UV-vis absorption is conducted in CH_2Cl_2 solution. [b] $E_{0\text{-}0}$ is extracted from the onset absorption wavelength. [c] E_{HOMO} calculated from the first-electron redox potentials, with an equation E_{HOMO}=-4.4-$E_{redox\text{-}1}$. The redox potentials were calibrated vs. standard hydrogen electrode (SHE) with $E_{(Fc/Fc+)}$ = 624 mV vs SHE as conversion. [d] $E_{LUMO}=E_{HOMO}+E_{0\text{-}0}$.

The PSCs based on the three HTMs were fabricated with a standard device configuration of FTO/TiO_2-underlayer/*meso*-TiO_2/perovskite/HTM/Au. **Figure 3a** shows the *J-V* curves of the PSCs based on different HTMs measured under 100 mWcm^{-2} AM 1.5 illumination. Surprisingly, we found that the device with HTM X41 showed very low photovoltaic performance with a PCE of <0.1% because of very low short-circuit current (J_{sc}) of 0.58 mAcm^{-2} and fill factor (*FF*) of 0.15. In contrast, AS37-based PSC demonstrated a PCE of 7.8% with J_{sc} of 20.05 mAcm^{-2}, V_{oc} of 1.06 V, and *FF* of 0.37. The device based on X44 showed highest performance with a PCE of 15.2% (J_{sc}=21.04 mAcm^{-2}, V_{oc}=1.08 V, and FF=0.67). The detailed photovoltaic parameters of the corresponding PSCs are shown in **Table 2**. For comparison, undoped spiro-OMeTAD was used as HTM in the PSCs with same conditions, and the as-obtained device showed a low PCE of 7.5% (J_{sc}=18.39 mAcm^{-2}, V_{oc}=1.08 V, and FF=0.38; see **Figure S8**), as reported in a similar recent publication by Zhang *et al.*[28] In order to understand the reasons for the lower performance for AS37 and X41 compared to that for X44, the dark current curves of the devices were recorded, as shown in **Figure 3b**. Since the dark current is mainly determined by the energy-level differences between the two contacts (TiO_2 and HTM) as well as the series resistance of the components in the devices, one can get information from dark current data on these aspects. By considering the fact that the three HTMs showed similar E_{HOMO} levels (see **Table 1**), the magnitude of the dark current could be mainly affected by the series resistance of HTM layer. As observed, X41-based device showed extremely low dark current compared to the PSCs with AS37 and X44. This is consistent with the fact that X41 has a low hole conductivity (8.95×10^{-5} Scm^{-1}), resulting in a high series resistance in the HTM layer which blocks the current flow through the X41-based capping layer in the device. AS37-based

PSC exhibited a much higher dark current compared to that of X41 in spite of their similar hole conductivities, which could be due to the formed pinholes in the HTM-AS37 layer causing some current leakage, as observed in **Figure 4b** and **4c**. As expected, X44-based device showed the highest dark current at high bias potentials which can be explained by its higher hole conductivity (9.03×10^{-5} Scm^{-1}).

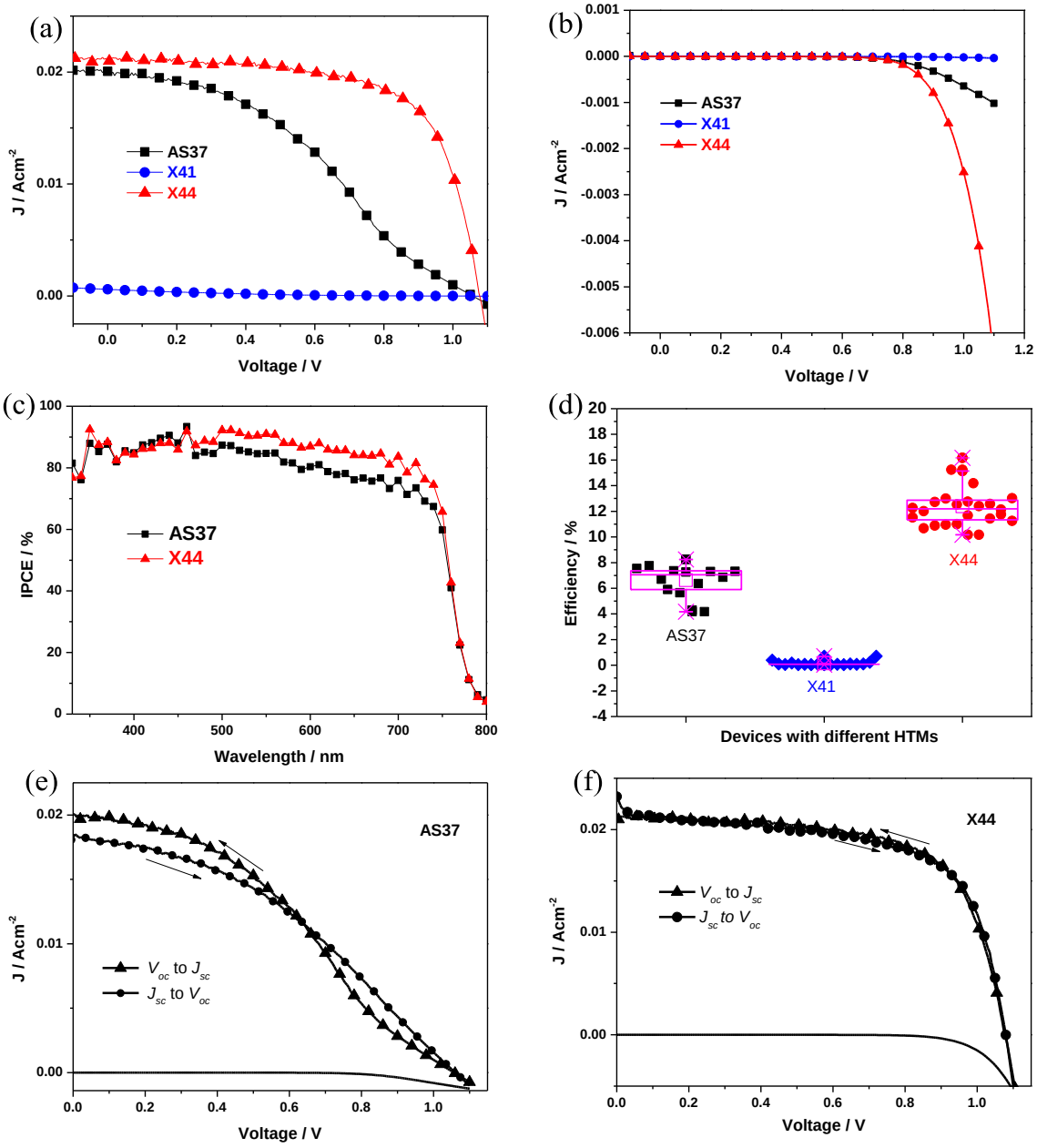

Figure 3. (a) *J-V* curves under light intensity of 100 $mWcm^{-2}$, (b) *J-V* curves in dark, (c) Incident Photon-to-current-conversion efficiency (IPCE) spectra, (d) device efficiency statistics for the devices based on HTM AS37, X41 and X44. (e) *J-V* curves at different scan directions of the devices based on AS37. (f) *J-V* curves at different scan directions of the devices based on X44.

Figure 3c shows the IPCE spectra of the devices with AS37 and X44. X44-based device has higher IPCE values than that for AS37-based devices, consistent with the higher J_{sc} obtained in X44-based PSCs. **Figure 3d** depicts the histogram of the performance of the obtained devices, confirming good reproducibility of PCEs. The current-voltage hysteresis behavior of the devices based on AS37 and X44 are shown in **Figure 3e** and **3f.** The details of the parameters are shown in **Table 2** and **Table S1**. It can be seen that the X44-based device exhibited very little hysteresis, while the hysteresis for the AS37-based device was more pronounced; a lower J_{sc} but a higher *FF* was obtained at the scan direction from V_{oc} to J_{sc} than those under the reverse scan. These effects could be related to the low hole conductivity of AS37, as reported previously.[29]

Table 2. Photovoltaic parameters of the devices based on undoped HTMs AS37, X41, X44 and spiro-OMeTAD.

HTM	η **/ %**	V_{oc} **/ mV**	J_{sc} **/ mAcm^{-2}**	***FF***
AS37	7.8	1.06	20.05	0.37
X41	0.08	0.92	0.58	0.15
X44	15.2	1.08	21.04	0.67
Spiro-OMeTAD	7.5	1.08	18.39	0.38

In order to obtain insights into the origins of the different photovoltaic performance for the devices based on the three HTMs, the morphological properties of the solid-state HTM films on the surface of perovskite were characterized in detail. As shown in **Figure 4a**, high-quality and pinhole-free mixed-ion perovskite ($[HC(NH_2)_2]_{0.85}(CH_3NH_3)_{0.15}Pb(I_{0.85}Br_{0.15})_3$) films are used in the devices. The perovskite film showed uniform grain size distribution with a diameter of ~200 nm. **Figure S9** exhibits the elemental analysis in the perovskite film, showing that the lead and halide ions (Br and I) are homogeneously dispersed in the whole perovskite film. **Figure 4b** and **4c** show the top view of the HTM AS37 layer deposited on top of the perovskite layer. The AS37 layer showed very rough and island-like aggregates. This may be attributed to its low glass-transition temperature, as observed in the previous work.[30] The ease of crystallization of AS37 results to its capping layer with poor uniformity and with many pinholes, which can affect the hole transport property as well as the perovskite protection from humidity.[31] Besides, the formed pinholes in AS37 film could allow some current flow, which could be the reason for the obtained higher dark current in the AS37-based device (see **Figure 3b**)

as well as the higher photovoltaic performance than that for X41-based device. However, the pinholes could enable some direct contact between Au and the perovskite, thereby resulting to a low shunt resistance and thus fast charge recombination in the device, as confirmed by the S-shaped *J-V* curve, and low *FF* of 0.37 for the AS37-based devices. In contrast, the X41 and X44 showed a much more uniform HTM capping layer. Both the capping layer compactness and low hole conductivity of X41 lead to a strong charge-conduction blocking effect and thus to poor solar-cell performance. Thus, it can be learnt that the molecular structural change from the alkyl chain to tertiary amine, and quaternary ammonium has a great impact on the uniformity of HTM capping layer.

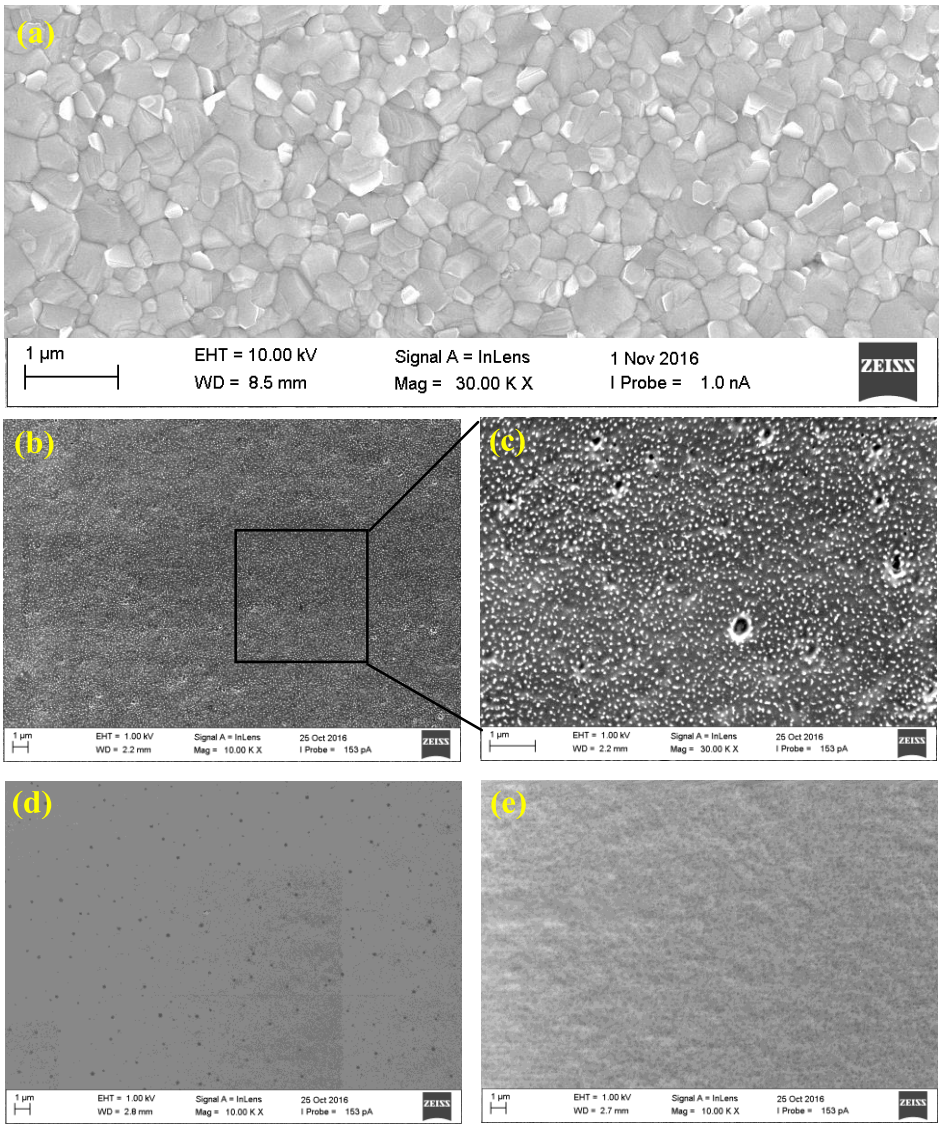

Figure 4. SEM image of the mixed-ion perovskite (a); and molecular morphology on the HTMs AS37 (b) and (c), X41 (d) and X44 (e).

As illustrated in **Figure 5a**, after light excitation of the perovskite-based light absorber, the hole-transfer process at the perovskite/HTM interface and charge transport in the bulk of HTM play a critical role in the charge collection and thus to the device performance. Since the only difference in the devices investigated here is the HTM layer, the device performance can be directly linked to the HTM properties.

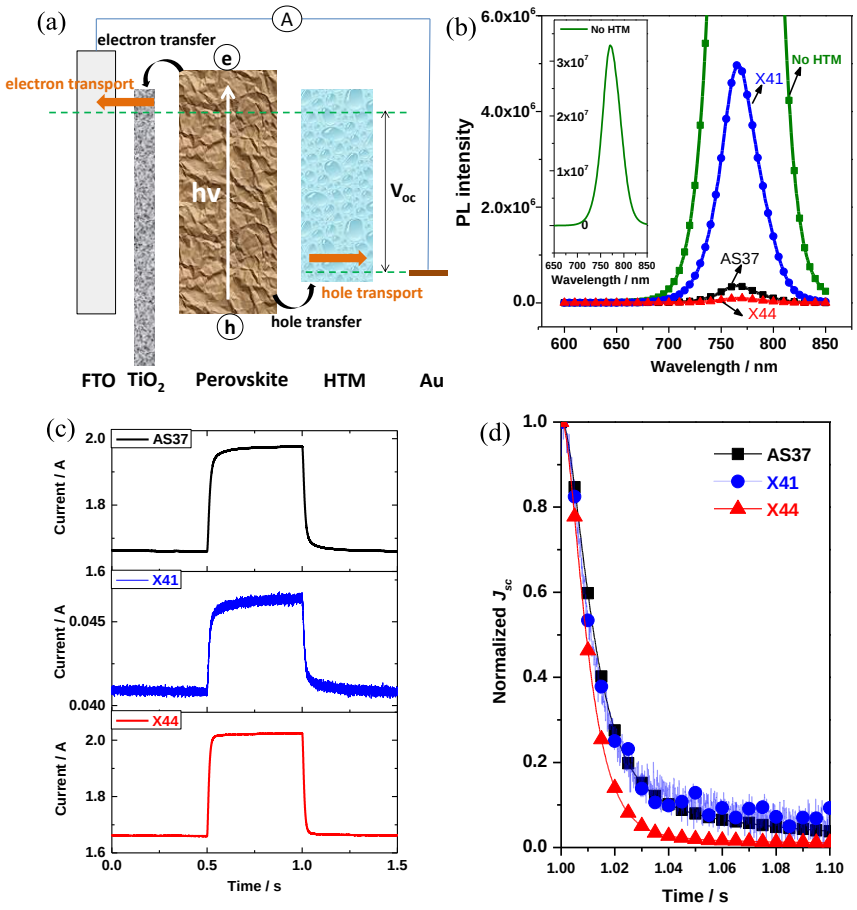

Figure 5. (a) Pathways of interfacial charge transfer and charge transport in the perovskite solar cells; (b) photoluminescence spectra of the electrode FTO/ZrO_2/perovskite with and without HTMs; (c) transient photocurrent rise and decay curves and (d) normalized transient photocurrent decay spectra.

Figure 5b shows the photoluminescence (*PL*) spectra of samples containing FTO/TiO_2/perovskite with and without HTM layer. The intensity of the *PL* can on the one hand give useful information on the yield of the radiative recombination and on the other hand reflects the efficiency of the charge transfer at the interfaces between perovskite and charge-selective layers. The substrate without the HTM layer demonstrated a very strong *PL* signal, meaning that the photogenerated charges recombine in the form of radiation. In contrast, after deposition of the HTM layer on perovskite, the *PL* intensity significantly

decreased, illustrating that the photo-induced charge carriers transfer to the contact materials so as to reduce the radiative recombination. Specifically, the X44-based substrate showed a very efficient *PL* quenching compared to that for AS37 or X41. Therefore, it can be concluded that a more efficient hole transfer at the perovskite/HTM interface occurs for X44 than AS37 and X41. The less efficient hole transfer for X41 compared to the other two HTMs could be one of the main reasons for the lower performance of the X41-based device. We suggest that the low hole-transfer yield for the X41-based device could be related to the strong electrostatic interaction between perovskite and the tertiary amines in X41, which may lead to a barrier for the interfacial hole transfer, as similarly found in one previous study that the tertiary amines and quaternary ammonium showed very different electrostatic binding property in biological applications.[32] In order to study the charge transport properties in the PSCs, transient photocurrent decay (TPCD) measurements were performed at the complete devices by applying a small-modulation light on top of a constant light intensity (100 $mWcm^{-2}$ in this work) illumination on the device at the short-circuit condition. By having this perturbation of light the photo-induced current rise and decay processes can be recorded with time, as shown in **Figure 5c**. By normalizing the TPCD curves, a qualitative comparison of the charge-extraction kinetics for the three HTMs is feasible. As shown in **Figure 5d**, the X44-based PSC showed faster photocurrent decay than the devices based on AS37 and X41, demonstrating that the charge extraction for X44 is far more efficient compared to the other two. The more efficient charge extraction in the X44-based device can explain the obtained higher J_{sc} and FF in PSCs with X44, as shown in **Figure 3a**. It can be suggested that this efficient charge extraction in the X44-based device is attributed to the high hole conductivity and uniform capping-layer formation capability of X44.

The long-term stability of the perovskite-based device is another important requirement for the future application of PSCs.[1, 33-34] Therefore, at first the stability of the devices based on X44 and AS37 at the maximum power point (MPP) condition was monitored, as shown in **Figure 6a, 6b, 6c**. It can be seen that the device with X44 shows very stable parameters of V_{mpp}, I_{mpp} and P_{mpp} and remain >90% of the initial performance after 1500s at MPP conditions (light intensity: 100 $mWcm^{-2}$). In contrast, the AS37-based device showed a fast degradation in all of V_{mpp}, I_{mpp} and P_{mpp}, so that >40% of the initial performance is lost under the same conditions. In addition, the long-term stability of the device was investigated with controlled aging conditions (room temperature and

<20% humidity in N_2 atmosphere in dark without encapsulation). AS37-based device maintained the photovoltaic performance by showing a PCE of 7.4% after 15 days compared to the initial PCE of 7.8%, but with improved *FF* and lower J_{SC}. The detailed parameters are listed in the inset table of **Figure 6d**. In comparison, the device with X44 showed a slight increase of efficiency from the initial 15.2% to 16.2% after 15 days with both improved J_{SC} and *FF* (see **Figure 6e**). It can be concluded that the ionic HTM X44 with counter ions showed promising stability in PSCs and holds a great potential for future applications.

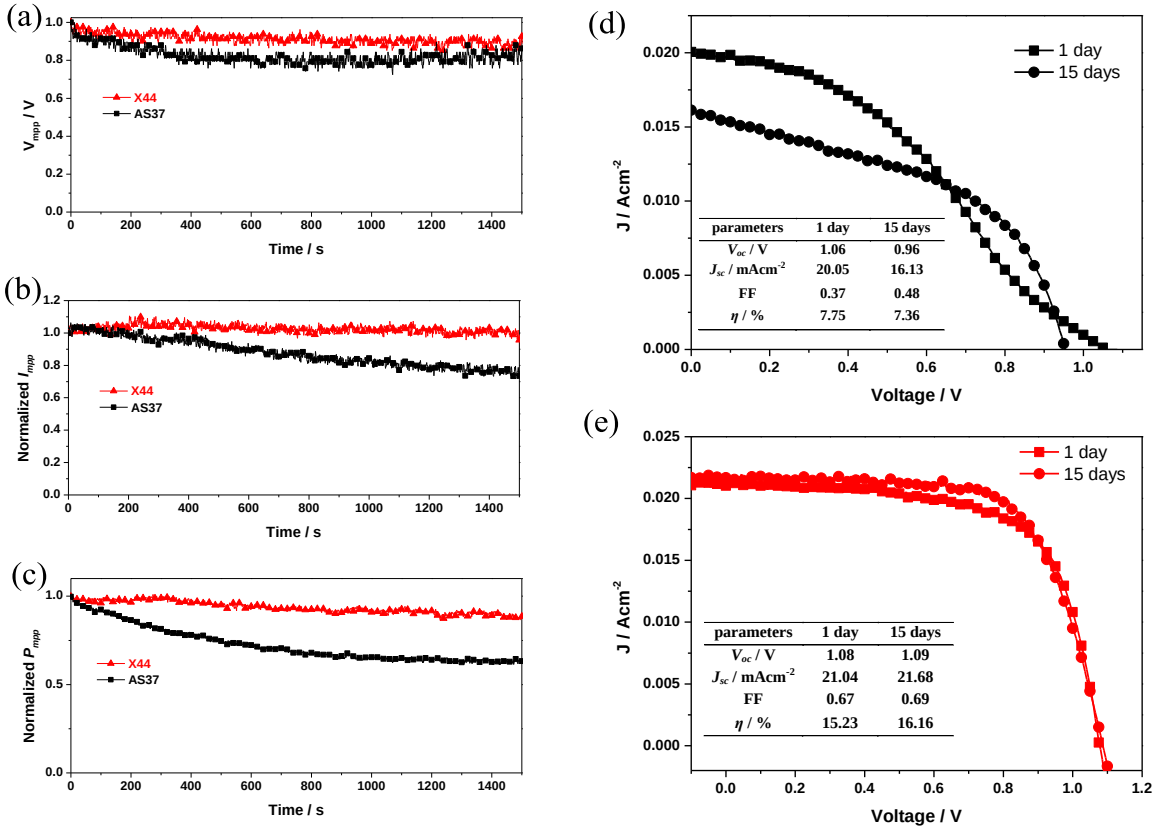

Figure 6. The device stability test under the maximum power point conditions by showing the change of V_{mpp} (a), J_{mpp} (b) and P_{mpp} (c). Long-term stability test of the PSCs in a controlled humidity (<20%) in dark without encapsulation after 15 days for AS37 (d) and X44 (e).

In conclusion, we have developed a new type of ionic organic molecule as dopant-free HTM for PSCs. Neither the light absorption properties nor energy level positioning of the molecules is not affected after the incorporation the ions in the molecules. However, by accompanying counter ions in the quaternary ammonium based molecule X44, the hole conductivity of X44 has been significantly improved (9.03×10^{-4} Scm^{-1}) compared to a tertiary amine-based reference molecule X41(8.95×10^{-5} Scm^{-1}) and its alkyl-chain based analogue

AS37 (7.65×10^{-5} Scm^{-1}). In contrast to the low performance of X41 and AS37 based devices with PCEs of 0.08% and 7.8%, respectively, this ionic molecule X44 has been successfully employed as dopant-free HTM in mixed-ion PSCs by exhibiting an impressive PCE of 16.2% after 15 days aging from an initial PCE of 15.2%. It has been observed that the counter ions in the molecule X44 presented great contributions to the more charge extraction in the device and also to the higher hole transfer yield at the interfaces. Besides, the device with HTM X44 demonstrated an impressive stability at MPP condition by maintaining more than 90% of initial performance. In addition, the PSC with X44 showed improved J_{sc} and *FF* after 15-days aging under controlled humidity without encapsulation. We believe this new strategy of designing ionic HTM via incorporation of counter ions will open one new promising way for developing efficient dopant-free HTMs for PSCs in the future.

Supporting Information

Supporting Information on experimental details, synthesis and characterization of HTMs is available from the Wiley Online Library or from the author.

Acknowledgements

Financial assistance has been provided by …

References

1. Federico Bella, G. G., Juan-Pablo Correa-Baena, Guido Saracco, Michael Grätzel, Anders Hagfeldt, Stefano Turri, Claudio Gerbaldi, Improving Efficiency and Stability of Perovskite Solar Cells with Photocurable Fluoropolymers. *Science* **2016**.
2. Heo, J. H., et al., Efficient Inorganic-Organic Hybrid Heterojunction Solar Cells Containing Perovskite Compound and Polymeric Hole Conductors. *Nat Photonics* **2013**, *7*, 487-492.
3. Michael Saliba1, T. M., Konrad Domanski1, Ji-Youn Seo, Amita Ummadisingu, Shaik M. Zakeeruddin, Juan-Pablo Correa-Baena, Wolfgang R. Tress, Antonio Abate, Anders Hagfeldt, Michael Grätzel, Incorporation of Rubidium Cations into Perovskite Solar Cells Improves Photovoltaic Performance. *Science* **2016**.
4. Saliba, M., et al., A Molecularly Engineered Hole-Transporting Material for Efficient Perovskite Solar Cells. *Nature Energy* **2016**, *1*, 15017.
5. Zhao, Y. X.; Zhu, K., Solution Chemistry Engineering toward High-Efficiency Perovskite Solar Cells. *J Phys Chem Lett* **2014**, *5*, 4175-4186.
6. Even, J.; Pedesseau, L.; Katan, C.; Kepenekian, M.; Lauret, J. S.; Sapori, D.; Deleporte, E., Solid-State Physics Perspective on Hybrid Perovskite Semiconductors. *J Phys Chem C* **2015**, *119*, 10161-10177.

7. Zhou, Z. M.; Pang, S. P.; Liu, Z. H.; Xu, H. X.; Cui, G. L., Interface Engineering for High-Performance Perovskite Hybrid Solar Cells. *J Mater Chem A* **2015**, *3*, 19205-19217.
8. Niu, G. D.; Guo, X. D.; Wang, L. D., Review of Recent Progress in Chemical Stability of Perovskite Solar Cells. *J Mater Chem A* **2015**, *3*, 8970-8980.
9. Kandada, A. R. S.; Petrozza, A., Photophysics of Hybrid Lead Halide Perovskites: The Role of Microstructure. *Accounts Chem Res* **2016**, *49*, 536-544.
10. Li, M. H.; Shen, P. S.; Wang, K. C.; Guo, T. F.; Chen, P., Inorganic P-Type Contact Materials for Perovskite-Based Solar Cells. *J Mater Chem A* **2015**, *3*, 9011-9019.
11. Yu, Z.; Sun, L., Recent Progress on Hole-Transporting Materials for Emerging Organometal Halide Perovskite Solar Cells. *Adv Energy Mater* **2015**, *5*, n/a-n/a.
12. Laura Calió, S. K., Michael Grätzel, Shahzada Ahmad, Hole-Transport Materials for Perovskite Solar Cells. *Angew Chem Int Ed Engl* **2016**.
13. Liu, J.; Pathak, S.; Stergiopoulos, T.; Leijtens, T.; Wojciechowski, K.; Schumann, S.; Kausch-Busies, N.; Snaith, H. J., Employing Pedot as the P-Type Charge Collection Layer in Regular Organic-Inorganic Perovskite Solar Cells. *J Phys Chem Lett* **2015**, *6*, 1666-73.
14. Zhang, J. B., et al., Constructive Effects of Alkyl Chains: A Strategy to Design Simple and Non-Spiro Hole Transporting Materials for High-Efficiency Mixed-Ion Perovskite Solar Cells. *Adv Energy Mater* **2016**, *6*.
15. Ameen, S.; Rub, M. A.; Kosa, S. A.; Alamry, K. A.; Akhtar, M. S.; Shin, H. S.; Seo, H. K.; Asiri, A. M.; Nazeeruddin, M. K., Perovskite Solar Cells: Influence of Hole Transporting Materials on Power Conversion Efficiency. *Chemsuschem* **2016**, *9*, 10-27.
16. Hua, Y.; Xu, B.; Liu, P.; Chen, H.; Tian, H.; Cheng, M.; Kloo, L.; Sun, L., High Conductivity Ag-Based Metal Organic Complexes as Dopant-Free Hole-Transport Materials for Perovskite Solar Cells with High Fill Factors. *Chem. Sci.* **2016**, *7*, 2633-2638.
17. Xu, B.; Huang, J.; Agren, H.; Kloo, L.; Hagfeldt, A.; Sun, L., Agtfsi as P-Type Dopant for Efficient and Stable Solid-State Dye-Sensitized and Perovskite Solar Cells. *Chemsuschem* **2014**, *7*, 3252-6.
18. Abate, A., et al., Lithium Salts as "Redox Active" P-Type Dopants for Organic Semiconductors and Their Impact in Solid-State Dye-Sensitized Solar Cells. *Phys Chem Chem Phys* **2013**, *15*, 2572-2579.
19. Yang, L.; Xu, B.; Bi, D. Q.; Tian, H. N.; Boschloo, G.; Sun, L. C.; Hagfeldt, A.; Johansson, E. M. J., Initial Light Soaking Treatment Enables Hole Transport Material to Outperform Spiro-Ometad in Solid-State Dye-Sensitized Solar Cells. *J Am Chem Soc* **2013**, *135*, 7378-7385.
20. Liao, H. C., et al., Dopant-Free Hole Transporting Polymers for High Efficiency, Environmentally Stable Perovskite Solar Cells. *Adv Energy Mater* **2016**, *6*.
21. Zhang, F., et al., Dopant-Free Star-Shaped Hole-Transport Materials for Efficient and Stable Perovskite Solar Cells. *Dyes Pigments* **2017**, *136*, 273-277.
22. Song, Y. K.; Lv, S. T.; Liu, X. C.; Li, X. G.; Wang, S. R.; Wei, H. Y.; Li, D. M.; Xiao, Y.; Meng, Q. B., Energy Level Tuning of Tpb-Based Hole-Transporting Materials for Highly Efficient Perovskite Solar Cells. *Chem Commun* **2014**, *50*, 15239-15242.
23. Wang, J. J.; Wang, S. R.; Li, X. G.; Zhu, L. F.; Meng, Q. B.; Xiao, Y.; Li, D. M., Novel Hole Transporting Materials with a Linear Pi-Conjugated Structure for Highly Efficient Perovskite Solar Cells. *Chem Commun* **2014**, *50*, 5829-5832.
24. Lv, S. T., et al., Mesoscopic Tio2/Ch3nh3pbi3 Perovskite Solar Cells with New Hole-Transporting Materials Containing Butadiene Derivatives. *Chem Commun* **2014**, *50*, 6931-6934.
25. Steck, C.; Franckevicius, M.; Zakeeruddin, S. M.; Mishra, A.; Bauerle, P.; Gratzel, M., A-D-a-Type S,N-Heteropentacene-Based Hole Transport Materials for Dopant-Free Perovskite Solar Cells. *J Mater Chem A* **2015**, *3*, 17738-17746.
26. Liu, J.; Wu, Y. Z.; Qin, C. J.; Yang, X. D.; Yasuda, T.; Islam, A.; Zhang, K.; Peng, W. Q.; Chen, W.; Han, L. Y., A Dopant-Free Hole-Transporting Material for Efficient and Stable Perovskite Solar Cells. *Energ Environ Sci* **2014**, *7*, 2963-2967.

27. Kim, G. W.; Kang, G.; Kim, J.; Lee, G. Y.; Kim, H. I.; Pyeon, L.; Lee, J.; Park, T., Dopant-Free Polymeric Hole Transport Materials for Highly Efficient and Stable Perovskite Solar Cells. *Energ Environ Sci* **2016**, *9*, 2326-2333.
28. Zhang, F., et al., A Novel Dopant-Free Triphenylamine Based Molecular "Butterfly" Hole-Transport Material for Highly Efficient and Stable Perovskite Solar Cells. *Adv Energy Mater* **2016**, *6*, 1600401.
29. Zhang, J., et al., Constructive Effects of Alkyl Chains: A Strategy to Design Simple and Non-Spiro Hole Transporting Materials for High-Efficiency Mixed-Ion Perovskite Solar Cells. *Adv Energy Mater* **2016**.
30. Leijtens, T.; Ding, I. K.; Giovenzana, T.; Bloking, J. T.; McGehee, M. D.; Sellinger, A., Hole Transport Materials with Low Glass Transition Temperatures and High Solubility for Application in Solid-State Dye-Sensitized Solar Cells. *Acs Nano* **2012**, *6*, 1455-1462.
31. Zhang, J.; Xu, B.; Johansson, M. B.; Vlachopoulos, N.; Boschloo, G.; Sun, L.; Johansson, E. M.; Hagfeldt, A., Strategy to Boost the Efficiency of Mixed-Ion Perovskite Solar Cells: Changing Geometry of the Hole Transporting Material. *Acs Nano* **2016**, *10*, 6816-25.
32. Saitoh, H.; Hasegawa, N.; Kawai, S.; Miyazaki, K.; Arita, T., Interaction of Tertiary-Amines and Quaternary Ammonium-Compounds with Gastrointestinal Mucin. *J Pharmacobio-Dynam* **1986**, *9*, 1008-1014.
33. Leo, K., Perovskite Photovoltaics: Signs of Stability. *Nat Nanotechnol* **2015**, *10*, 574-5.
34. Berhe, T. A.; Su, W.-N.; Chen, C.-H.; Pan, C.-J.; Cheng, J.-H.; Chen, H.-M.; Tsai, M.-C.; Chen, L.-Y.; Dubale, A. A.; Hwang, B.-J., Organometal Halide Perovskite Solar Cells: Degradation and Stability. *Energy Environ. Sci.* **2015**.